THE ASTROPHYSICAL JOURNAL, 367:593–600, 1991 February 1

RESONANT INTERACTION IN COMMON ENVELOPES

NOAM SOKER

Harvard-Smithsonian Center for Astrophysics
Received 1990 May 29; accepted 1990 July 26

ABSTRACT

The resonant interaction between an orbiting low-mass secondary star and the pulsational modes of the primary in a common envelope binary system is studied. When the secondary is very close to the envelope, and especially if it is inside the envelope, i.e., the system is in a common envelope phase, a rich spectrum of both *g*- and *p*-modes can be excited. During the common envelope phase high-order and high harmonic *p*-modes become important. By means of a simple one-zone model, the amplitudes of the forced oscillations are approximately estimated. It is claimed that if several conditions are met, then a brown dwarf secondary can cause nonnegligible axisymmetrical mass loss through its resonant interaction with a red giant primary's envelope. One implication of this for elliptical planetary nebulae is discussed.

Subject headings: stars: binaries — stars: pulsation

I. INTRODUCTION

It is widely believed now that a common envelope (CE) phase occurs in the course of the evolution of most binary stars with separation of $r_2 \lesssim 1000\ R_\odot$ and total mass of approximately 1 $M_\odot$ or more. The massive star of the two, the primary, expands substantially as it evolves to become a red giant and engulfs the lower mass companion, the secondary. Even if the initial separation is larger than the giant radius (but by no more than a factor of a few; this factor depends on the masses), tidal forces are very efficient in bringing the two stars closer (Livio and Soker 1983). The CE evolution is assumed to reduce the separation of wide binaries and transform them into close binaries, unless the secondary is evaporated in the envelope or collides with the primary core (Livio and Soker 1984*a*). Accordingly, the CE is supposed to lead to the formation of cataclysmic variables (Paczyński 1976; Eggleton 1986), some low-mass X-ray binaries (e.g., 2A 0620−00; Eggleton and Verbunt 1986), and double white dwarf systems that are supposed to be the progenitors of Type I supernovae (e.g., Webbink and Iben 1987).

As discussed by Livio and Soker (1988), despite its wide applicability, very few actual calculations of the CE phase exist. One of the reasons is the absence of spherical or cylindrical symmetry in the problem. The two-dimensional (Bodenheimer and Taam 1984; Taam and Bodenheimer 1989) and three-dimensional (Livio and Soker 1988) hydrodynamic calculations demonstrate the importance of taking into account two- and three-dimensional effects. These calculations find a high-velocity flow in the equatorial plane as a result of the secondary interaction with the envelope. In addition, the secondary interacts with the matter in its immediate surroundings via accretion and drag forces (e.g., Taam, Bodenheimer, and Ostriker 1978; Livio and Soker 1984*a*). The energy released from these processes is deposited into the envelope and contributes to the system's luminosity. All these processes are important for massive companions and are not subjects of the current work.

Another outcome of the CE evolution was proposed on different grounds, in cases where the primary is a moderate-mass red giant. It has been proposed that the asymmetrical mass flow mentioned above (Soker and Livio 1989) or the deposition of orbital angular momentum into a red giant envelope (Soker 1990) can cause an enhanced mass loss in the equatorial plane, which can then lead to the formation of an elliptical planetary nebula (Balick 1987). The likelihood of this scenario is supported by study of specific nebulae: Mendez *et al.* (1988) proposed a collision of the secondary with the giant core during the CE phase in two planetary nebulae, 125−47 1 and 212+23 1. Plait and Soker (1990) discuss the CE evolution as a plausible scenario to explain the spherically symmetric outer halo and elliptical inner region of the planetary nebula NGC 6826.

In the present work we carry out a preliminary study of yet another process which takes place during the CE phase, and which can cause an asymmetrical mass loss; we study the basic nature of the excitation of stellar pulsations by a low-mass secondary orbiting inside the envelope. The resonant interaction in binaries has been discussed in many contexts in the past, but mainly regarding the secondary outside the primary envelope. This was done, for example, by Savonije and Papaloizou (1983, hereafter SP) in their study of tidal interactions in detached binaries (i.e., the secondary is outside the envelope). In § II we illustrate the rich spectrum of modes that can be resonantly excited at many different radii of the secondary, when it is inside or very close to the primary surface.

This kind of interaction has no spherical symmetry. By decomposing the gravitational potential of the secondary to spherical harmonics, however, ordinary differential equations can be obtained. In principle the same equations that were used by SP, and which are given in § III, describe the interaction in the CE stage. In the current work, however, we do not integrate the equations to obtain full accurate solutions, as we plan to do in a following work, but rather explore the nature of resonant interaction during the CE stage. For this purpose we use a simple model to solve the equations, and we derive a qualitative description of nonadiabatic oscillations (§ IV). In § V we summarize and discuss future works to elaborate and apply the results of this work.

II. RADII OF RESONANT EXCITATION

a) General Discussion

Nonradial stellar oscillations can in principle be divided into *p*-, *g*-, and *f*-modes (Cox 1980, § 17.7). (However, for stellar models with a large central mass concentration the low-order modes are no longer pure; Scuflaire 1974.) The *p*-waves are

characterized by a large radial (relative to the transverse) displacement and by large Eulerian pressure and density amplitudes. The g-waves are predominantly transverse and have small Eulerian pressure and density amplitudes. The amplitude of the p-modes is small in the inner region of the star, becoming larger close to the stellar surface. The g-modes, on the other hand, can have large amplitudes in the inner region. Moreover, the frequencies of the p-modes are determined mainly by conditions in the outer stellar regions, and those of the g-modes by conditions in the deeper stellar interior (Cox 1980, § 17.13). We expect, therefore, that if stellar pulsations lead to enhanced mass loss it would mainly be through p-wave oscillations.

The presence of the secondary star inside the giant's envelope changes the nature of the interaction between the two stars, as compared with detached binaries. First, since the distance between the secondary and the core of the primary is smaller than the primary radius, high-order harmonics of the secondary's potential (§ III) cannot be neglected. Thus, for example, McMillan, Taam, and McDermott (1990), in their calculations of the companion outside the primary envelope, could consider only the $l \leq 4$ harmonics in the potential, neglecting higher orders, while SP consider only the $l = 2$ harmonic. This cannot be done in the CE stage. Moreover, the $l = 1$ modes cannot be regarded as a constant acceleration of the whole primary (Kopal 1959, § II.1) but should be treated as a real mode of oscillation (see Cox 1980, § 17.8, for discussion of the $l = 1$ modes). Second, the short orbital period can efficiently excite p-waves. In the case of detached binaries, mainly the g-waves are excited.

Along this line, we focus in this section on finding the companion's radii r_2 at which resonant excitations are likely to take place. By means of three simple approaches it is shown that p-waves are much more likely to be excited when the secondary is inside the envelope of the primary than when it is outside. Radii for p-mode resonant excitations are more common for low orders (small n) and high-degree spherical harmonics (high-l modes).

b) *The Homogeneous Compressible Model*

For the purpose of this section, which is to find the radii r_2 at which resonantly excited pulsations in a CE can occur, it is adequate and very convenient to start with the unrealistic homogeneous compressible stellar model (Cox 1980, § 17.7). Because we take the secondary to be a low-mass star, we assume that the structure of the primary does not change as it enters the CE phase. The linear adiabatic eigenfrequencies σ of the homogeneous compressible stellar model are given by (Pekeris 1938; Cox 1980, eq. [17.77])

$$\Omega^2(l, n) = D \pm [D^2 + l(l+1)]^{1/2} , \qquad (2.1)$$

where $\Omega^2 \equiv \sigma^2 R^3/GM$, with R, M, G being the stellar radius, the stellar mass, and the gravitational constant, respectively. The quantity D is defined by

$$D = -2 + 0.5\Gamma_1[n(2l + 2n + 5) + 2l + 3] , \qquad (2.2)$$

where $n = 0, 1, 2, \ldots$ is the order of the mode, l is the spherical harmonic degree, and Γ_1 is the adiabatic exponent. The plus sign in equation (2.1) gives the p-modes, and the minus sign the g-modes. In addition, there are the f-modes with frequencies (Chandrasekhar 1964; Cox 1980, eq. [17.80])

$$\Omega_f^2(l) = \frac{2l(l-1)}{2l+1} . \qquad (2.3)$$

The potential of a point mass orbiting the primary center at a constant distance r_2 can be decomposed into spherical harmonics Y_{lm} (§ III), each having a frequency

$$\Omega_2 = \left(\frac{R}{r_2}\right)^{3/2} m , \quad |m| = l, l-2, l-4, \ldots , \qquad (2.4)$$

where it is assumed that all the mass of the primary is inner to r_2. The mass of the secondary will be neglected from now on.

The lowest frequency p-modes are those with $n = 0$, which for $\Gamma_1 = 3/2$ are $\Omega_p^2(l, n = 0) = 0.5[0.5 + 3l + (13l^2 + 7l + 0.25)^{1/2}]$. This gives $\Omega_p^2 = 10.6$ and 13.9 for $l = 3$ and $l = 4$, respectively. For a companion outside the envelope $r_2 > R$, only p-modes with $l \geq 4$ can be excited, as can be seen by substituting $m = l$ in equation (2.4). In Table 1 the radii at which p-wave resonances occur, that is, when the frequency given by equation (2.1) with the plus sign is equal to that given in equation (2.4), are given for $\Gamma_1 = 5/3$ and $l \leq 10$. Also presented is the radius-dependent factor in the potential $(R/r_2)^{l+1}$ (see eq. [3.8]). There are 12 radii of resonance in Table 1; for $\Gamma_1 = 4/3$ and $l \leq 10$ there are 16 radii of resonance, and for $l < 20$ with $\Gamma_1 = 5/3$ there are 105 radii of resonance. Among the latter, however, the largest radius for which $(R/r_2)^{l+1} > 0.01$ is $r_2 = 1.436R$ for $(l, m) = (11, 11)$, and the largest for which $(R/r_2)^{l+1} > 0.1$ is $r_2 = 1.286R$ for $(l, m) = (8, 8)$. These results demonstrate that p-waves are more likely to be excited when the companion is very close to, or inside, the stellar surface. From Table 1 it can be seen that high-order modes (high n) can be excited at small radii for sufficiently high l, and that, for the same order n, higher spherical harmonics are excited at larger radii, as is also demonstrated in § II*d*.

In the homogeneous model the orbital period for $r_2 < R$ is the same as for $r_2 = R$. In more realistic stellar models the orbital frequency increases as the companion gets closer to the center, and more modes can be resonantly excited, as is shown in the next subsection.

c) *Dependence on Stellar Model: $l = 2$ Modes in Polytropic Models*

As the stellar model becomes more centrally mass-concentrated, the orbital frequency increases more rapidly as the secondary gets deeper into the envelope. This allows more p-modes to be resonantly excited. To demonstrate this behavior, we use the frequencies of the first 10 orders of $l = 2$ modes for several different polytropic models as given by Cox (1980, Table 17.2). The orbital frrequency at each radius, which was

TABLE 1

p-MODE RESONANT RADII FOR THE HOMOGENEOUS MODEL

r_2/R	$(R/r_2)^{l+1}$	n	l	m
1.389.....	0.027	0	10	10
1.340.....	0.054	0	9	9
1.286.....	0.104	0	8	8
1.228.....	0.193	0	7	7
1.197.....	0.138	0	10	8
1.164.....	0.346	0	6	6
1.133.....	0.286	0	9	7
1.091.....	0.591	0	5	5
1.074.....	0.455	1	10	10
1.062.....	0.582	0	8	6
1.031.....	0.736	1	9	9
1.008.....	0.960	0	4	4

TABLE 2

RESONANT RADII FOR $l = 2$ IN POLYTROPIC MODELS

		n									
v	MODE	1	2	3	4	5	6	7	8	9	10
1.....	p	0.577	...	...	...	...	...	...	...	...	...
2.....	p	0.673	0.432	0.176	...	...	...	...	...	...	...
3.....	p	0.634	0.514	0.427	0.359	0.300	0.248	0.198	0.147	0.085	...
	g	0.934	...	...	...	...	...	...	...	...	...
	f	0.787	...	...	...	...	...	...	...	...	...
4.....	p	0.454	0.426	0.396	0.369	0.352	0.330	0.307	0.286	0.268	0.251
	g	0.524	0.558	0.605	0.638	0.679	0.735	0.791	0.845	0.899	0.951
	f	0.487	...	...	...	...	...	...	...	...	...

calculated by solving for the appropriate polytropic model, was multiplied by $m = 2$ to get the exciting frequency for the $l = 2$ modes. The homogeneous stellar model corresponds to $v = 0$, where v is the polytropic index. For this model we saw that the $l = 2$ p-modes cannot be resonantly excited. The secondary radii, in units of the stellar radius R, at which resonances occur for the first 10 g- and p-modes and for the f-mode, are given in Table 2 for four polytropic indices v. (Note that here, and in general, $n = 1$ is the lowest mode, whereas in the homogeneous compressible model $n = 0$ is the lowest mode.)

Table 2 clearly demonstrates the rich spectrum of resonant excited $l = 2$ modes and the large number of the secondary radii at which this resonant interaction can take place. For the $l = 2$ modes, as the primary becomes more centrally mass-concentrated, the g-modes are more likely to be resonantly excited than the p-modes when the secondary is close to the surface. As can be seen from Table 1, and Table 3 below, higher degree (higher l) p-modes can be resonantly excited when the secondary is closer to the surface. The p-mode frequencies do not change much as we move toward more mass-concentrated models (higher v). The p_6 mode, for example, has frequencies of $\Omega^2_{p6} = 129.9$ and 105.2 for the $v = 1$ and $v = 4$ models, respectively. The g-modes, on the other hand, are unstable in the $v = 1$ polytropic model, with frequencies of $\Omega^2_{g6} = 0.7188$ and 10.08 in the $v = 3$ and $v = 4$ models, respectively.

d) Very High Order p-Modes

The very high order modes are those for which $l \gg 1$ and/or the wavelength is much shorter than the pressure scale height. A discussion of these modes, together with their oscillation frequencies, can be found, e.g., in Cox (1980, § 17.12). We assume in this section that the stellar model is very concentrated, that is, most of the mass is in a small core, so that equation (2.4) for the secondary frequencies can be used at any radius. We further assume that in the relevant region we can write $P = P_0 r^{-q}$, so that in hydrostatic equilibrium $GM/r = qP/\rho$. By using equation (2.4) for Ω_2, the expression for high-order p-modes (e.g., Cox 1980, eq. [17.95]) can be written as

$$\Omega_p^2 \simeq \frac{l(l+1) + (rk)^2}{m^2} \frac{\Gamma_1}{q} \left(\frac{r_2}{r}\right)^3 \Omega_2^2 , \qquad (2.5)$$

where $k = 2\pi/\lambda_r$ is the radial wavenumber and λ_r is the radial wavelength. At resonance $\Omega_p = \Omega_2$, and it occurs at radii

$$\frac{r_2}{r} \simeq \left[\frac{m^2}{l(l+1) + (rk)^2}\right]^{1/3} \left(\frac{q}{\Gamma_1}\right)^{1/3} . \qquad (2.6)$$

Since for typical stellar models $(q/\Gamma_1)^{1/3} \lesssim 2$, resonances for large rk will occur mainly for $r_2 \lesssim r$, which can be the case only while the companion is inside the primary envelope. To illustrate the behavior of r_2/r as given by equation (2.6), this quantity is given in Table 3, for two values of rk, 6π, and 4π, and for $(q/\Gamma_1)^{1/3} = 1.5$ (note that in Table 3 r_2/r is given, and not r_2/R as in Tables 1 and 2). Only modes with $l \leq 10$ and $(r_2/r)^l > 0.1$ [or, if $r_2 > r$, $(r/r_2)^{l+1} > 0.1$] for $rk = 4\pi$ are presented. If higher values of l are allowed, more p-modes appear with r_2 close to r. Thus, for example, for $l \leq 20$ and $rk = 4\pi$ under the same constraints, there are 47 radii of resonance, as compared with 12 in Table 3. This demonstrates again the rich spectrum of excited modes.

So far we have been concerned only with secondary radii at which resonant excitations can occur. We turn now to calculation of the amplitudes of the nonadiabatic response. In the present work we use a simple model to estimate the response approximately. We start by writing the basic equations.

III. BASIC EQUATIONS

a) The Linear Nonadiabatic Equations

In this subsection we write the equations which describe the nonadiabatic response to the companion potential of Eulerian linear perturbations of the primary. We adopt the Cowling approximation, i.e., the perturbation to the gravitational potential caused by the stellar response is neglected. The equations are basically the same as those used by SP, with the difference that here the secondary's potential will be for a circular orbit and for arbitrary Y_{lm}. We will therefore not repeat the

TABLE 3

RESONANT RADII FOR HIGH-ORDER p-MODES

	$rk = 4\pi$		$rk = 6\pi$	
(l, m)	r_2/r	$(r_2/r)^l$	r_2/r	$(r_2/r)^l$
(10, 10)	1.080	0.429[a]	0.898	0.343
(9, 9)	1.033	0.722[a]	0.850	0.231
(8, 8)	0.979	0.847	0.797	0.162
(10, 8)	0.931	0.488	0.774	0.0775
(7, 7)	0.918	0.549	0.738	0.119
(9, 7)	0.874	0.297	0.719	0.0512
(6, 6)	0.847	0.369	0.674	0.0935
(8, 6)	0.808	0.183	0.658	0.0350
(5, 5)	0.766	0.263	0.603	0.0796
(7, 5)	0.733	0.114	0.590	0.0248
(4, 4)	0.672	0.204	0.524	0.0754
(3, 3)	0.563	0.179	0.436	0.0827
(2, 2)	0.435	0.189	0.334	0.112
(1, 1)	0.276	0.276	0.211	0.211

[a] These values are $(r/r_2)^{l+1}$

derivation, but rather give the final form. The Eulerian perturbation vector variables are the stellar displacement $\boldsymbol{\xi} = (\xi_r, \xi_\theta, \xi_\phi)$ and the energy flux $\boldsymbol{F}' = (F'_r, F'_\theta, F'_\phi)$. The Eulerian scalar variables are the pressure P', density ρ', temperature T', and opacity κ'. Quantities without primes represent the unperturbed stellar variables. We separate each of ξ_r, P', ρ', T', and F'_r into the form $\xi_r(r, \theta, \phi) = \xi_r(r) Y_{lm}(\theta, \phi) e^{-i\sigma t}/|Y_{lm}(\pi/2, \phi)|$, etc. In this form $\xi_r(r)$, and the radial parts of the other variables, are the amplitude in the equatorial plane $\theta = \pi/2$. By eliminating ξ_θ, ξ_ϕ, F'_θ, F'_ϕ and canceling $Y_{lm}(\theta, \phi)e^{-i\sigma t}/|Y_{lm}(\pi/2, \phi)|$, we obtain the desired equations for the radial-dependent part of each variable (SP):

$$-\sigma^2 \xi_r = -\frac{1}{\rho}\frac{dP'}{dr} + \frac{\rho'}{\rho^2}\frac{dP}{dr} - \frac{d\Phi_{lm}}{dr}, \tag{3.1}$$

$$\frac{1}{\rho}\frac{d}{dr}(r^2 \rho \xi_r) = -r^2 \frac{\rho'}{\rho} + \frac{l(l+1)}{\sigma^2}\left(\frac{P'}{\rho} + \Phi_{lm}\right), \tag{3.2}$$

$$\frac{P'}{P} - \Gamma_1 \frac{\rho'}{\rho} + A\xi_r = i\eta\left[-\frac{1}{Fr^2}\frac{d}{dr}(r^2 F'_r) + \frac{l(l+1)}{r^2}\left(\frac{d\ln T}{dr}\right)^{-1}\frac{T'}{T}\right], \tag{3.3}$$

$$\frac{F'_r}{F} = \left(\frac{d\ln T}{dr}\right)^{-1}\frac{d}{dr}\frac{T'}{T} + (4 - \kappa_T)\frac{T'}{T} - (1 + \kappa_\rho)\frac{\rho'}{\rho}, \tag{3.4}$$

where

$$A = \frac{d\ln P}{dr} - \Gamma_1 \frac{d\ln \rho}{dr}, \tag{3.5}$$

$$\kappa_T = \left(\frac{\partial \ln \kappa}{\partial \ln T}\right)_\rho, \quad \kappa_\rho = \left(\frac{\partial \ln \kappa}{\partial \ln \rho}\right)_T, \tag{3.6}$$

and

$$\eta \equiv \frac{(\Gamma_3 - 1)F}{\sigma P} \tag{3.7}$$

is a characteristic radiative diffusion length scale (SP); Γ_1 and Γ_3 are the adiabatic exponents (e.g., Cox 1980). Near the surface η/R is large, and the response is highly nonadiabatic, whereas in the stellar interior it is small and the response is adiabatic (see § IV). Φ_{lm} is defined in the next subsection.

The limitation of the above set of equations should be kept in mind throughout the rest of this paper. The energy equation (3.3) and the radiative transfer equation (3.4) are applicable only in the radiative transfer diffusion approximation. Thus, they do not hold above the photosphere or in convective regions. However, since the set of equations will be solved approximately to derive an illustrative solution, we will discuss the results in a more general sense.

b) *The Perturbing Potential*

The potential at $\boldsymbol{r}$ due to the secondary at $\boldsymbol{r}_2$ is written in terms of spherical harmonics (e.g., Jackson 1975):

$$\frac{-GM_2}{|\boldsymbol{r} - \boldsymbol{r}_2|} = -GM_2 \sum_{l=0}^{\infty}\sum_{m=-l}^{l}\frac{4\pi}{2l+1}\frac{r_<^l}{r_>^{l+1}} Y_{lm}(\theta, \phi) Y^*_{lm}(\theta_2, \phi_2)$$
$$= \sum_{l=0}^{\infty}\sum_{m=-l}^{l}\Phi_{lm}\frac{Y_{lm}(\theta, \phi)}{|Y_{lm}(\pi/2, \phi)|}e^{-i\sigma t}, \tag{3.8}$$

where $r_>$ ($r_<$) is the greater (lesser) of r and r_2. We take the circular orbit to be in the plane $\theta_2 = \pi/2$ with $\phi_2 = t(GM/r_2^3)^{1/2}$, so that $\sigma = m(GM/r_2^3)^{1/2}$ is the forcing frequency, with M being the total mass inner to r_2. Equation (3.8) defines Φ_{lm}, which can be written as

$$\Phi_{lm} = -\frac{GM}{r_>}\left(\frac{r_<}{r_>}\right)^l \frac{M_2}{M}\frac{(l-m)!}{(l+m)!}[P_l^m(0)]^2, \quad m > 0, \tag{3.9}$$

where P_l^m is the associated Legendre function of degree l and order m. If the primary star does not rotate, the mode $(l, -m)$ is symmetric to the mode (l, m). Thus, when the real parts of the amplitudes of the two modes are combined, the final amplitude is twice that given by each mode. In § IV, therefore, the potential is taken to be $2\Phi_{lm}$, and the solution is given for $m > 0$.

c) *Power-Law Atmosphere*

In the next section we approximate a shell inside the stellar envelope by a power-law profile and assume that the amount of mass in the shell is negligible compared with the interior mass. For a power-law density profile $\rho \propto r^{-d}$ and with all the mass being interior to the shell and the secondary orbit, we then derive

$$\frac{P}{\rho} = \frac{r^2\sigma_0^2}{d+1}, \quad rA = (\Gamma_1 - 1)d - 1, \quad \frac{\sigma^2}{\sigma_0^2} = m^2\left(\frac{r}{r_2}\right)^3, \tag{3.10}$$

where A is defined in equation (3.5) and

$$\sigma_0^2 \equiv \frac{GM}{r^3} = -\frac{1}{r\rho}\frac{dP}{dr}. \tag{3.11}$$

The linearized equation of state (which is necessary to close the set of equations [3.1]–[3.4]) to be used in the next section is taken to be

$$\frac{P'}{P} = \frac{\rho'}{\rho} + \frac{T'}{T}. \tag{3.12}$$

The exponent of the power-law density profile d is not an independent parameter, but rather depends on other physical parameters in the envelope. In the diffusion limit the density profile exponent and the exponents of the opacity coefficient are related though

$$3 - \kappa_T = d(1 + \kappa_\rho). \tag{3.13}$$

IV. A SIMPLIFIED SOLUTION: BAKER'S ONE-ZONE MODEL

a) *The Equations for the One-Zone Model*

As a first approach, for an approximate estimate of the amplitudes of forced oscillations, we apply the one-zone model used by Baker for stability analysis of radial modes (Baker 1966). In addition, we are using the assumptions mentioned in § IIIc. The solutions we derived here should be considered more as a qualitative description than as a quantitative one.

In Baker's model the behavior of a single spherical shell of mass Δm is studied. Here we take the shell's thickness to be $\Delta r \ll r$. The essential assumptions are that all the physical variables and all relative Lagrangian perturbations, except for the luminosity, are constant in space throughout the shell. Under the assumption of power-law profiles for the unperturbed physical variables, we find that the Eulerian variables are also constant throughout the shell:

$$\frac{d}{dr}\left(\frac{p'}{P}\right) = \frac{d}{dr}\left(\frac{T'}{T}\right) = \frac{d}{dr}\left(\frac{\rho'}{\rho}\right) = 0. \tag{4.1}$$

The perturbation in luminosity incident on the inner boundary of the shell is assumed to be zero, and the value of this perturbation in the shell is taken to be half that value in the outer boundary. The derivative of the perturbed luminosity is then given by (Baker 1966)

$$\frac{d}{dr}\left(\frac{L'}{L}\right)=\frac{2}{\Delta r}\left(\frac{L'}{L}\right). \tag{4.2}$$

Using equations (4.1) and (4.2) for the derivatives of the perturbations and equation (3.11) for σ_0 in the linear equations (3.1) and (3.2), and substituting for L'/L in equation (3.3) from equation (3.4), we obtain a set of algebraic equations

$$-\sigma^2\xi_r=\left(\frac{P'}{P}-\frac{\rho'}{\rho}\right)r\sigma_0^2-\frac{d\Phi_{lm}}{dr}, \tag{4.3}$$

$$\xi_r\frac{d\ln\rho}{dr}+3\frac{\xi_r}{r}=-\frac{\rho'}{\rho}+\frac{l(l+1)}{r^2\sigma^2}\left(\frac{P'}{\rho}+\Phi_{lm}\right), \tag{4.4}$$

$$\frac{P'}{P}-\Gamma_1\frac{\rho'}{\rho}+A\xi_r=i\eta\left\{\frac{2}{\Delta r}\left[(1+\kappa_\rho)\frac{\rho'}{\rho}-(4-\kappa_T)\frac{T'}{T}\right]+\frac{l(l+1)}{r^2}\left(\frac{d\ln T}{dr}\right)^{-1}\frac{T'}{T}\right\}. \tag{4.5}$$

By substituting for T'/T from the equation of state (3.12), eliminating ρ'/ρ and P'/P using the assumption of a power-law atmosphere (§ IIIc), and using expression (3.9) for the perturbing potential, we derive the equation for the displacement amplitude:

$$C\frac{\xi_r}{r}=2\Phi_{lm}\frac{l(l+1)}{r^2\sigma^2}\times\begin{cases}D_2-\dfrac{1}{l}D_1, & r_2\le r,\\ D_2+\dfrac{1}{(l+1)}D_1, & r_2>r,\end{cases} \tag{4.6}$$

where

$$\mathrm{Re}\ C=4-3\Gamma_1+\frac{\sigma^2}{\sigma_0^2}+\frac{\sigma_0^2}{\sigma^2}\left(\frac{\Gamma_1 d}{d+1}-1\right)l(l+1)-\frac{\Gamma_1}{d+1}l(l+1), \tag{4.7}$$

$$\mathrm{Im}\ C=\beta\frac{\sigma_0}{\sigma}(d-3)(1+\kappa_\rho)+\mathrm{Im}\ D_1, \tag{4.8}$$

$$\mathrm{Re}\ D_1=\frac{\sigma^2}{\sigma_0^2}-\frac{\Gamma_1}{d+1}l(l+1), \tag{4.9}$$

$$\mathrm{Im}\ D_1=-\beta\frac{\sigma_0}{\sigma}\left\{\frac{l(l+1)}{d+1}(1+\kappa_\rho)+\left[(\kappa_T-4)-\frac{\Delta r}{2r}l(l+1)\right]\left[\frac{\sigma^2}{\sigma_0^2}-\frac{l(l+1)}{d+1}\right]\right\}, \tag{4.10}$$

$$\mathrm{Re}\ D_2=1-\Gamma_1, \tag{4.11}$$

$$\mathrm{Im}\ D_2=-\beta\frac{\sigma_0}{\sigma}(1+\kappa_\rho), \tag{4.12}$$

$$\beta\equiv\frac{\sigma}{\sigma_0}\frac{2\eta}{\Delta r}=\frac{2}{\Delta r}\frac{(\Gamma_3-1)F}{\sigma_0 P}, \tag{4.13}$$

and "Re" and "Im" stand for the real and imaginary parts, respectively. Note that in the current model $(\sigma/\sigma_0)^2=m^2(r/r_2)^3$ and that the factor 2 in equation (4.6) is due to the symmetry of the (l, m) and $(l, -m)$ modes.

b) Some Properties of the One-Zone Model

We assume now that the one-zone shell is in the very outer region of the star. For a widely separated binary $r_2 \gg r$, the $(l, m) = (2, 2)$ mode dominates, and the equilibrium displacement is given by $\xi_r/r=(\frac{3}{4})(M_2/M)(r/r_2)^3$. In order to obtain this limit, we must take $d\to\infty$, which, by equation (3.13) and the demand that κ_T be finite, requires $\kappa_\rho=-1$. For a high value of d in the adiabatic limit Re C is always positive, and thus no resonances exist. In Figure 1 the amplitudes of the displacement for three adiabatic modes are presented, for $M_2/M=0.01$ and $\Gamma_1=5/3$. The most prominent character of the amplitudes is the change in sign at $r_2=r$ and then at $r_2/r=1.26$ for the $(l, m)=(2, 2)$ mode and at $r_2/r=1.5$ for the $(l, m)=(3, 3)$ mode. The (3, 1) mode always has a positive displacement. A positive displacement at $r_2<r$ and a negative one at $r_2>r$ mean that the segment of the shell closest to the secondary is displaced away from the secondary. At large r_2 the displacement is positive for all modes. When the secondary is at a large distance from the primary, the forcing frequency is low and the envelope can adjust itself to the forcing potential; the potential term Φ_{lm} in equation (3.1) prevails over the force term $d\Phi_{lm}/dr$ in equation (3.2). Thus, the primary surface in the secondary's direction rises toward the secondary. When the secondary is close to the envelope, the forcing frequency is high and the force term dominates over the potential term. In this case the displacement is such that maximum secondary force, that is, when the secondary is the closest, corresponds to maximum acceleration of the shell. This results in the displace-

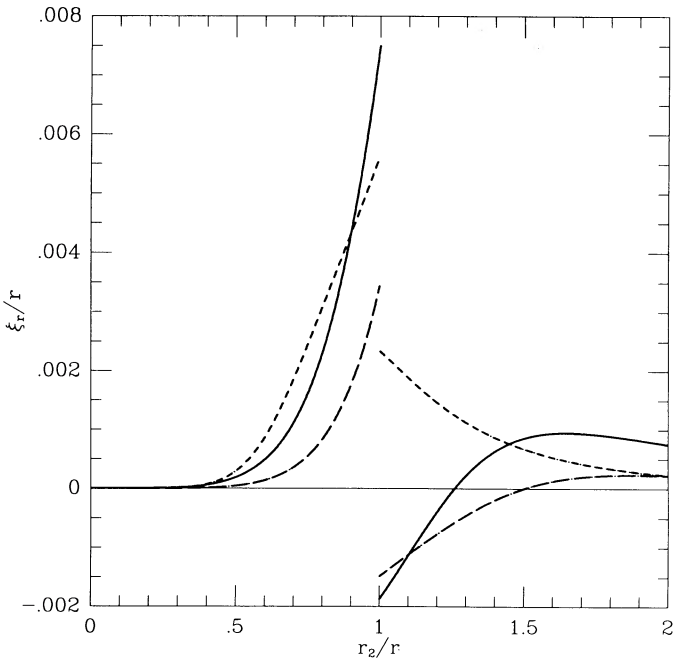

FIG. 1.—Amplitudes of the radial displacement in the equatorial plane (in units of the shell radius r), for a secondary mass of $M_2=0.01M$, shown as a function of the secondary orbital radius. The density profile in the shell has an infinite slope, $d\to\infty$, and the response is adiabatic. Plotted are results for the modes $(l, m)=(2, 2)$, (3, 1), and (3, 3) shown by solid, short-dashed and long-dashed curves, respectively.

ment being away from the secondary. From the $r_2 > r$ right-hand side of equation (4.6) we find that the change of behavior occurs at $r_2 = \{m^2/[(\Gamma_1 - 1)(l + 1)]\}^{1/3}$.

To gain more insight into the one-zone model we examine adiabatic oscillations, i.e., $\beta = 0$, with no external potential, i.e., $\Phi_{lm} = 0$. Thus we are left with the equation Re $C = 0$, where σ now is any frequency σ_f. In the case of radial modes $l = 0$, and we recover the equation obtained by Baker for this case $\sigma_f = \sigma_0(3\Gamma_1 - 4)^{1/2}$. For the adiabatic nonradial modes we take the homogeneous model $d = 0$, for which σ_0 is constant throughout the stellar model, so that $\sigma_f/\sigma_0 = \Omega_f$, and we obtain the equation

$$\Omega^4 + \Omega^2[4 - 3\Gamma_1 - \Gamma_1 l(l + 1)] - l(l + 1) = 0 . \quad (4.14)$$

Comparing this with the accurate results for the homogeneous model (e.g., Cox, 1980. eq. [17.76; eq. [2.1] in this paper), we find that the two solutions are identical if

$$n = \tfrac{1}{4}[-5 - 2l + (12l^2 + 12l + 25)^{1/2}] . \quad (4.15)$$

For most l-values, n will not be an integer, whereas, in the accurate solution, $n = 0, 1, 2, \ldots$. In any case, it is still interesting to give several values of n calculated from equation (4.15). We find that the one-zone homogeneous model adiabatic frequencies with $l = 1$, (3), (6), 13, 24, (50), 188, 341 correspond to modes in the accurate solution having the same values of l, and $n = 0$, (0.5), (1.5), 4. 8, (17.5), 68, 124, respectively, where parentheses enclose the values for the noninteger n. The assumption of the perturbed variables being constant throughout the shell limits the one-zone model to low-order modes.

Let us look now at forced oscillations. A simple expression for the radii of resonances in the adiabatic limit can be obtained from equation (4.6) by taking $\Gamma_1 d = d + 1$. In the adiabatic limit resonances occur when Re $C = 0$, which by equation (4.7) reads

$$\frac{r_2}{r} = \left[\frac{m^2}{l(l + 1) + q(3\Gamma_1 - 4)/\Gamma_1}\right]^{1/3}\left(\frac{q}{\Gamma_1}\right)^{1/3} , \quad (4.16)$$

where, as in this section, r is the radius of the shell, and $q = d + 1$ is the power-law index of the pressure. This expression has the same form as the one derived for very high order p-modes in equation (2.6), if we identify $(rk)^2 = q(3\Gamma_1 - 4)/\Gamma_1$. For $\Gamma_1 = 5/3$, $q = 5/2$ and $rk = (3/2)^{1/2}$. We see that under the above assumption for the relation between Γ_1 and d the one-zone model corresponds to very low-order modes.

The last two examples considered in this section suggest that the one-zone model, though highly limited, is adequate for studying the basic nature of low-order mode forced oscillations.

c) *The Amplitudes of the Forced Oscillations*

In the one-zone model the nonadiabatic amplitude of ξ_r/r depends on $\Delta r/r$, Γ_1, d, κ_T, κ_ρ, and β. We give here results for an illustrative model with $\Delta r/r = 0.1$, $\Gamma_1 = 5/3$, $d = 2.5$, $\kappa_T = 0$, and thus by equation (3.13) $\kappa_\rho = 0.2$. We present the results for the amplitudes of the displacement $|\xi_r/r|$, calculated from equation (4.6), as a function of the secondary orbital radius r_2/r for a secondary mass of $M_2/M = 0.01$. Since the $l = 1$ mode corresponds to a uniform acceleration of the mass inner to r_2 (see § IIa), this mode is limited to $r_2 < r$. The discontinuity in all graphs at $r_2/r = 1$ results from the discontinuity in the derivative of Φ_{lm} there (see eq. [4.6]).

TABLE 4

RESONANT RADII AND AMPLITUDES IN THE ONE-ZONE MODEL

	$\beta = 0.01$		$\beta = 20$	
(l, m)	r_2/r	$\lvert\xi_r/r\rvert$	r_2/r	$\lvert\xi_r/r\rvert$
(1, 1)	0.833	0.526	...	...
(2, 2)	1.042	0.181	1.197	0.142
(3, 1)	0.540	0.0283	0.608	0.0172
(3, 3)	1.123	0.108	1.264	0.0377
(5, 3)	0.845	0.0303	0.948	0.0116
(5, 5)	1.188	0.0320	1.333	4.10×10^{-3}
(7, 5)	0.971	0.0261	1.097	2.11×10^{-3}
(7, 7)	1.216	9.78×10^{-3}	1.373	6.54×10^{-4}
(9, 5)	0.832	2.50×10^{-3}	0.947	1.05×10^{-3}
(9, 7)	1.041	9.13×10^{-3}	1.185	3.75×10^{-4}
(9, 9)	1.231	3.22×10^{-3}	1.402	1.33×10^{-4}
(10, 8)	1.065	5.15×10^{-3}	1.218	1.73×10^{-4}

In Figure 2*a* we present results for an almost adiabatic case with $\beta = 0.01$. The $(l, m) = (3, 1)$ adiabatic mode shows two resonances, the inner one being the p-mode and the outer one the g-mode. In the adiabatic limit resonances occur when Re $C = 0$, which generally has two solutions for σ^2 and thus two radii at which resonance occurs. The $(l, m) = (2, 2)$ adiabatic g-mode resonance, for example, occurs at $r_2 = 2.31r$, which is outside the range of Figure 2*a*. Several examples of higher modes are shown in Table 4 with the radii of the p-mode resonances given in the second column (the radii are given for the adiabatic case $\beta = 0$; the values for $\beta = 0.01$ are practically the same) and the amplitude at each radius in the third column.

In the highly nonadiabatic limit ($\beta \to \infty$) resonances occur when Im $C = 0$, which has only one solution. The results for a highly nonadiabatic case are presented for $\beta = 20$ in Figure 2*b* for the first four modes, and in Table 4 for several higher modes. The resonant amplitudes in the highly nonadiabatic case decrease faster than those in the adiabatic limit as we ascend to higher modes. This is because higher frequencies (which result from higher values of m) make the response less nonadiabatic due to the factor $\beta\sigma_0/\sigma$ in equation (4.6).

In the limit of very high l, the ratio of the p-mode resonant radii in the adiabatic case to that of the highly nonadiabatic case of the same mode is $\Gamma_1^{-1/3}$. This results from the decrease of the sound speed from its adiabatic value $(\Gamma_1 P/\rho)^{1/2}$ to its isothermal value $(P/\rho)^{1/2}$ (Unno *et al.* 1989, § 23), and from the forcing frequency being proportional to $r^{-3/2}$. In the current case this ratio for very high l is 0.843. For lower values of l the above ratio is closer to unity, as can be seen in Table 4.

In an intermediate case, which is presented in Figure 2*c* for $\beta = 1$, there are no resonances but, rather, broad peaks. For these kinds of intermediate cases we do not expect that resonant interaction will be important. Thus, there might be stellar models for which no strong resonant interaction will take place. This will be studied in greater detail in a future work.

Although the displacement amplitude decreases rapidly as we ascend to higher modes, this is not true for the velocity amplitude, which decreases more slowly for high m. The amplitude of the radial velocity in the equatorial plane which corresponds to a mode (l, m) is given by

$$|V_r| = \frac{m}{\sqrt{2}}\frac{|\xi_r|}{r}\left(\frac{r}{r_2}\right)^{3/2} V_{\rm esc} , \quad (4.17)$$

where $V_{\rm esc}$ is the escape velocity from r. Thus, high-m modes

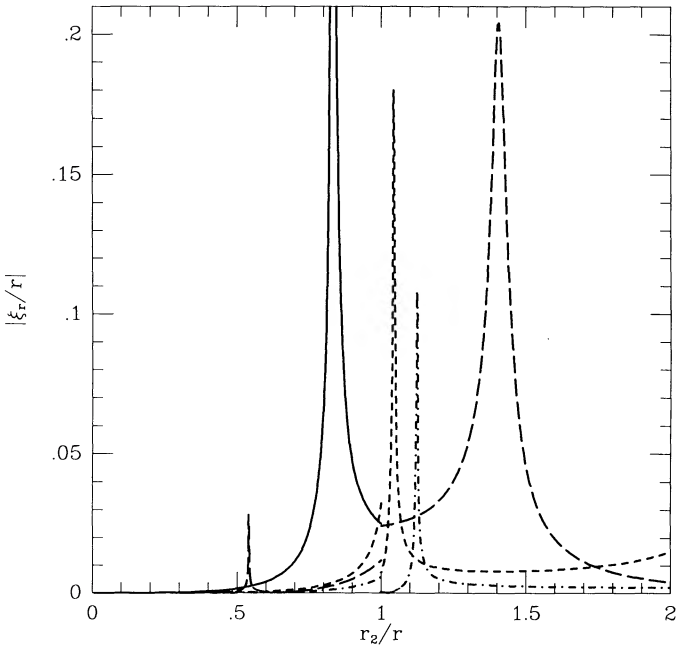

FIG. 2*a*

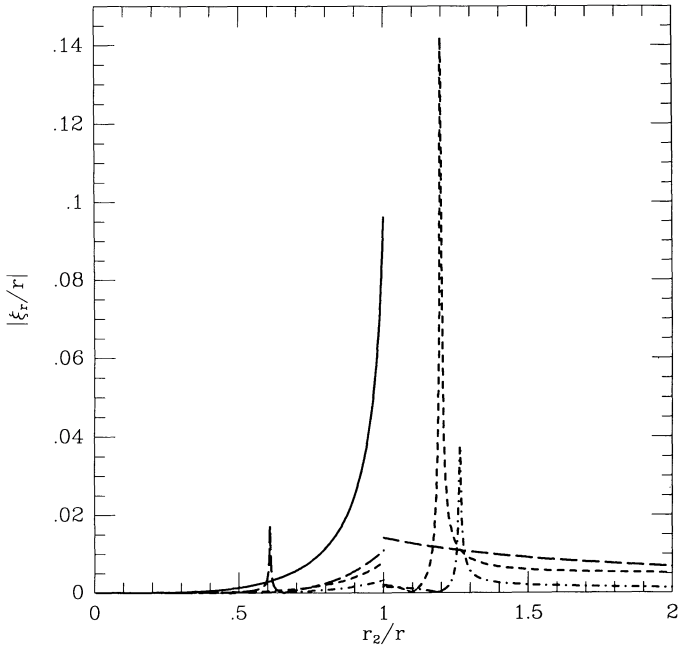

FIG. 2*b*

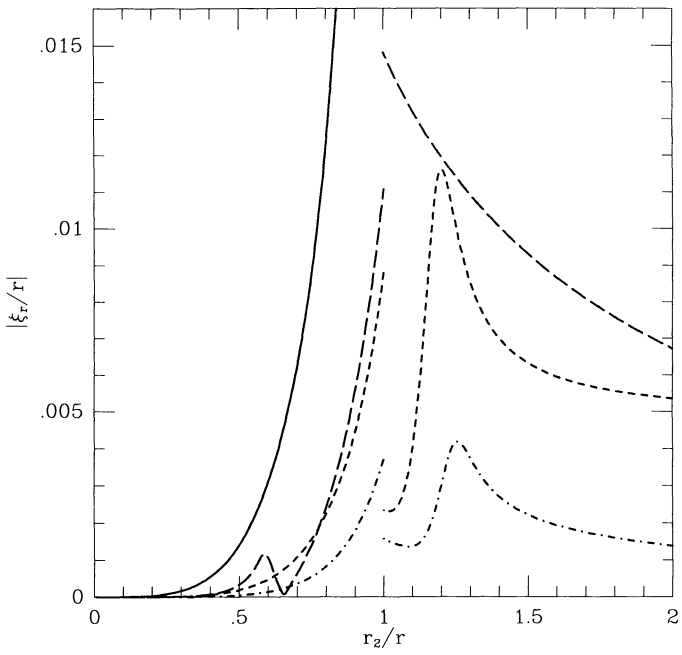

FIG. 2*c*

FIG. 2.—Amplitudes of the radial displacement in the equatorial plane (in units of the shell radius r), for a secondary mass of $M_2 = 0.01M$, shown as a function of the secondary orbital radius. The physical parameters of the shell are given in the text. Plotted are results for the modes $(l, m) = (1, 1), (2, 2), (3, 1)$, and (3, 3) shown by solid, short-dashed, long-dashed, and dot-dash curves, respectively. (*a*) Almost adiabatic case $\beta = 0.01$. (*b*) Highly nonadiabatic case $\beta = 20$. (*c*) $\beta = 1$. The amplitude of the $(l, m) = (1, 1)$ mode in Fig. 2*c* reaches a maximum of 0.0643 at $r_2 = r$.

can have large velocity amplitudes as compared with their displacement amplitudes.

The amplitudes which are calculated in the one-zone model need not be the same ones as at the surface of the star. In a realistic stellar model we do not expect the response of the envelope to be limited to a well-defined thin zone. It is more likely that global modes would be present, or that the waves would propagate in a large zone. The amplitudes of p-modes are increasing toward the stellar surface. Thus, if the amplitudes calculated in this section are appropriate for an inner zone, the amplitude at the surface can be much larger. Considering the limitations of the one-zone model, the main conclusion from the results presented in Figure 2 can be stated as follows: For highly nonadiabatic or highly adiabatic oscillations the response of the envelope to the forcing secondary potential can be very strong, and a low-mass companion ($M_2/M \sim 10^{-2}$) can cause a nonnegligible effect on the envelope. We discuss one implication of this in the next section.

From Figure 2 we see that the amplitudes depend on the values of β and $\Delta r/r$. The dependence on $\Delta r/r$ is the limitation of the one-zone model, while the dependence on β is more general. A word of caution should be said here concerning nonadiabatic effects. In the red giant phase most of the envelope (with the exception of a thin outer ragion) is convective, while the equations used in this work are written for a radiative transfer. Livio and Soker (1984*b*), in their calculations of a brown dwarf inside a red giant, used a red giant model with 0.88 $M_\odot$ and 400 $R_\odot$, in which the outer 40 $R_\odot$ is a radiative region (Harpaz 1984). Taking the outer radiative region to be the one-zone shell, we have $r = 380\ R_\odot$ and $\Delta r = 40\ R_\odot$. We find that a good fit to the density profile in the outer radiative region is $d = 15$, and since the temperature and density are very low in this region, $\kappa_T \simeq \kappa_\rho \simeq 0$. These last three values, however, do not satisfy equation (3.13). This is because the diffusion approximation breaks down in this tenuous outer region. In any event, with the above values and other values appropriate for that model, we find that $\beta \simeq 200$. This high value of β means that the response of the outer region is highly nonadiabatic, as expected for outer regions of stars (e.g., SP).

V. SUMMARY

The goal of this paper is to illustrate the importance of resonant interaction during the common envelope phase of

binaries with low-mass secondaries. The rich spectrum of modes that can be excited at many different orbits of the secondary, inside and close to the primary surface, was demonstrated in § II through Tables 1–3. As the secondary gets closer to the primary, higher degree p-modes (higher l) become important. The one-zone model was used to get an approximate estimate for the displacement amplitude of the forced oscillations. As illustrated in Figure 2, this response can be very strong for high and low β-values.

The common envelope phase with low-mass secondaries is very likely to take place when the primary is a red giant. The resonant interaction might influence the mass loss of the primary to be axisymmetric, with an enhanced mass loss in the equatorial plane, which might eventually lead to the formation of an elliptical planetary nebula (Balick 1987). Massive secondaries can cause asymmetrical mass loss through their direct interaction with the envelope, as was demonstrated in hydrodynamical simulations (Bodenheimer and Taam 1984; Livio and Soker 1988; Taam and Bodenheimer 1989), and by deposition of angular momentum into the red giant envelope (Soker 1990). Brown dwarf secondaries with masses $M_2 \gtrsim 0.02M$ can cause axisymmetric mass loss by transferring orbital angular momentum into rotation of the red giant (Soker 1990).

We showed in this work that brown dwarfs with masses $M_2/M \gtrsim 10^{-2}$ can resonantly excite oscillation modes in the primary envelope, and thus might cause equatorial enhanced mass loss. This last effect will be nonnegligible if the interaction takes place during the high mass loss phase of the red giant and if the forced oscillations enhance mass loss. (The connection between the pulsation and mass loss is beyond the scope of the current work.) This mechanism for an axisymmetric mass loss implies that elliptical planetary nebulae, if they are a result of such a mass-loss profile, can have a very low mass brown dwarf, which is beyond the current detection limit, orbiting around the central mass. Such binaries in the centers of elliptical planetary nebulae as a result of angular momentum transfer are discussed by Soker (1990).

The current preliminary study is an illustrative one. Several points should be elaborated in future works. First, the observational implications of resonant interaction during the common envelope phase, i.e., a way to detect such systems and to attribute this mechanism to known systems, is being studied (Whitney, Clayton, and Soker 1990). Second, a study of high-order modes in the WKB approximation, somewhat similar to the approach used by Balbus and Soker (1990) in studying the resonant interaction of a galaxy in the intracluster medium, can teach us a lot. Finally, a full integration of the equations in order to deal with global modes is essential for the understanding of the process. The last two approaches require a detailed stellar model, where there is the additional complication of the convective envelope in red giants.

I thank Martin Laming for a careful reading of the manuscript of this paper, and Mario Livio and Bob Noyes for helpful discussions. I also thank the referee for his comments, which made this manuscript more clear.

REFERENCES

Baker, N. 1966, in *Stellar Evolution*, ed. R. F. Stein and A. G. W. Cameron (New York: Plenum), p. 333.
Balbus, S. A., and Soker, N. 1990, *Ap. J.*, **357**, 353.
Balick, B. 1987, *A.J.*, **94**, 671.
Bodenheimer, P., and Taam, R. E. 1984, *Ap. J.*, **280**, 771.
Chandrasekhar, S. 1964, *Ap. J.*, **139**, 664.
Cox, J. P. 1980, *Theory of Stellar Pulsations* (Princeton: Princeton University Press).
Eggleton, P. P. 1986, in *The Evolution of Galactic X-Ray Binaries*, ed. J. Trümper, W. H. G. Lewin, and W. Brinkmann (Dordrecht: Reidel), p. 87.
Eggleton, P. P., and Verbunt, F. 1986, *M.N.R.A.S.*, **220**, 12P.
Harpaz, A. 1984, *M.N.R.A.S.*, **210**, 633.
Jackson, J. D. 1975, *Classical Electrodynamics* (New York: Wiley).
Kopal, Z. 1959, *Close Binary Systems* (New York: Wiley).
Livio, M., and Soker, N. 1983, *Astr. Ap.*, **125**, L12.
———. 1984*a*, *M.N.R.A.S.*, **208**, 763.
———. 1984*b*, *M.N.R.A.S.*, **208**, 783.
———. 1988, *Ap. J.*, **329**, 764.
McMillan, S. L. W., Taam, R. E., and McDermott, P. N. 1990, *Ap. J.*, **354**, 190.
Mendez, R. H., Groth, H. G., Husfeld, D., Kudritzki, R. P., and Herrero, A. 1988, *Astr. Ap.*, **197**, L25.
Paczyński, B. 1976, in *IAU Symposium 73, Structure and Evolution of Close Binary Systems*, ed. P. Eggleton, S. Mitton, and J. Whelan (Dordrecht: Reidel), p. 75.
Pekeris, C. L. 1938, *Ap. J.*, **88**, 189.
Plait, P., and Soker, N. 1990, *A.J.*, **99**, 1883.
Savonije, G. J., and Papaloizou, J. C. B. 1983, *M.N.R.A.S.*, **203**, 581 (SP).
Scuflaire, R. 1974, *Astr. Ap.*, **36**, 107.
Soker, N. 1990, *A.J.*, **99**, 1869.
Soker, M., and Livio, M. 1989, *Ap. J.*, **339**, 268.
Taam, R. E., and Bodenheimer, P. 1989, *Ap. J.*, **337**, 849.
Taam, R. E., Bodenheimer, P., and Ostriker, J. P. 1978, *Ap. J.*, **222**, 269.
Unno, W., Osaki, Y., Ando, H., Saio, H., and Shibahashi, H. 1989, *Nonradial Oscillations of Stars* (Tokyo: University of Tokyo Press).
Webbink, R. F., and Iben, I., Jr. 1987, in *IAU Colloquium 95, Second Conference on Faint Blue Stars*, ed. A. G. D. Philip, D. S. Hayes, and J. Liebert (Schenectady: Davis), p. 445.
Whitney, B. A., Clayton, G. C., and Soker, N. 1990, in preparation.

NOAM SOKER: Mail Stop 15, Center for Astrophysics, 60 Garden Street, Cambridge, MA 02138